MOLECULAR AND CELLULAR BIOLOGY, Dec. 1998, p. 7455–7465 Vol. 18, No. 12
0270-7306/98/$04.00+0

Strain-Dependent Myeloid Hyperplasia, Growth Deficiency, and Accelerated Cell Cycle in Mice Lacking the Rb-Related *p107* Gene

JENNIFER E. LECOUTER, BORIS KABLAR, W. RODNEY HARDY, CHUYAN YING, LYNN A. MEGENEY, LINDA L. MAY, AND MICHAEL A. RUDNICKI*

Institute for Molecular Biology and Biotechnology, McMaster University, Hamilton, Ontario, Canada L8S 4K1

Received 19 May 1998/Returned for modification 30 June 1998/Accepted 28 August 1998

To investigate the function of the Rb-related *p107* gene, a null mutation in *p107* was introduced into the germ line of mice and bred into a BALB/cJ genetic background. Mice lacking *p107* were viable and fertile but displayed impaired growth, reaching about 50% of normal weight by 21 days of age. Mutant mice exhibited a diathetic myeloproliferative disorder characterized by ectopic myeloid hyperplasia in the spleen and liver. Embryonic $p107^{-/-}$ fibroblasts and primary myoblasts isolated from adult $p107^{-/-}$ mice displayed a striking twofold acceleration in doubling time. However, cell sort analysis indicated that the fraction of cells in G_1, S, and G_2 was unaltered, suggesting that the different phases of the cell cycle in $p107^{-/-}$ cells was uniformly reduced by a factor of 2. Western analysis of cyclin expression in synchronized $p107^{-/-}$ fibroblasts revealed that expression of cyclins E and A preceded that of D1. Mutant embryos expressed approximately twice the normal level of Rb, whereas p130 levels were unaltered. Lastly, mutant mice reverted to a wild-type phenotype following a single backcross with C57BL/6J mice, suggesting the existence of modifier genes that have potentially epistatic relationships with *p107*. Therefore, we conclude that *p107* is an important player in negatively regulating the rate of progression of the cell cycle, but in a strain-dependent manner.

The Rb family of structurally related nuclear phosphoproteins, consisting of Rb, p107, and p130, is believed to play important roles in regulating cell proliferation and differentiation (42). A central function of the Rb family is to negatively regulate the activity of E2F transcription factors that control the transcription of many cell cycle-regulated genes (41). Cyclin-dependent kinases (cdks) differentially regulate the phosphorylation of Rb, p107, and p130 during the cell cycle. Consequently, different Rb family members are hypophosphorylated during different phases of the cell cycle, allowing the formation of complexes that contain specific E2F transcription factors (10–13, 21, 55).

The E2F family of transcription factors is encoded by multiple genes (at least six E2Fs and three DP-type members) and can regulate the transcription of many different genes that are putatively activated or repressed by specific E2F:DP heterodimers (26). Rb family–E2F1-5:DP complexes are believed to bind promoters at E2F sites and inhibit transcription by binding HDAC1, a histone deacetylase, to repress gene expression via chromatin remodeling (8, 36, 37) or, alternatively, to interfere with functional interactions between transactivation domains and components of the basal transcriptional machinery (9, 53). Thus, different E2F-regulated genes can be either activated or repressed depending on whether E2F:DP or an Rb family–E2F:DP complex is bound. Presumably, it is the cyclic activation and repression of E2F-regulated genes that controls progression through the cell cycle (41, 62).

The phenotype of mice carrying targeted mutations in *Rb* supports the assertion that *Rb* is intimately involved in cell differentiation and tumorigenesis. Homozygous mutant embryos die in utero between days 13.5 and 15.5 of gestation and exhibit defects in erythropoiesis and extensive cell death in the central nervous system (13, 25, 31). Chimeras containing both wild-type (WT) and *Rb*-deficient cells are viable but exhibit adrenal medulla hyperplasias, pituitary tumors, and lens cataracts (25, 63). Unlike *Rb*-deficient embryos, $Rb^{-/-}$:wild-type chimeras contain mature *Rb*-deficient erythrocytes, suggesting that erythroid cell differentiation is delayed rather than blocked in the absence of Rb.

Mice lacking either *p107* or *p130* in a mixed 129/Sv:C57BL/6J genetic background exhibit no overt phenotype and are viable and fertile, and embryonic fibroblasts (EF) derived from the mutants display normal cell cycle kinetics (14, 24, 32). Embryos lacking both *Rb* and *p107* die in utero 2 days earlier than *Rb*-deficient embryos and exhibit apoptosis in the liver and central nervous system, suggesting some redundancy in function. Compound mutant mice lacking both *p130* and *p107* die soon after birth and exhibit defective endochondral bone development due to a deficiency in chondrocyte differentiation. Taken together, these data suggested that p107 and p130 have relatively subtle roles in regulating the cell cycle and that a significant degree of overlap in function between the proteins exists (14, 32).

We have independently derived a targeted null mutation in *p107* into the germ line of mice. In our experiments, we bred chimeras with mice from the BALB/cJ strain. Surprisingly, we observed that mice lacking *p107* displayed growth deficits, a diathetic myeloproliferative disorder, and accelerated cell cycle kinetics. These data strongly support the assertion that *p107* in a BALB/cJ genetic background plays an essential role in negatively regulating the overall length of the cell cycle. Moreover, the observed strain dependence of the phenotype suggests the existence of second-site modifier genes that have potentially epistatic relationships with *p107*.

* Corresponding author. Mailing address: Institute for Molecular Biology and Biotechnology, McMaster University, Hamilton, Ontario, Canada L8S 4K1. Phone: (905) 525-9140, ext. 27424. Fax: (905) 521-2955. E-mail: rudnicki@mcmaster.ca.

MATERIALS AND METHODS

Generation of *p107* mutant mice. The replacement type *p107* targeting vector contains the PGK-neomycin cassette inserted into a *Bam*HI site immediately downstream of the codon encoding amino acid (aa) 165 of the *p107* gene in the reverse transcriptional orientation (see Fig. 1). The *p107* targeting vector was linearized with *Not*I, and gene targeting was performed with the J1 line of ES cells as described previously (51). The J1 line of ES cells is derived from the 129/Sv strain of mice (33). Targeting events were detected by Southern analysis of *Eco*RI-digested genomic DNA by using probe A and were confirmed by using probe B on *Hin*dIII-digested DNA. Two independent targeted lines were injected into BALB/cJ blastocyst stage embryos to generate chimeras. Chimeras were subsequently mated to BALB/cJ females, and the resulting heterozygous mice were bred to produce homozygous mutant mice. Care of animals was in accordance with institutional guidelines.

Northern and immunoblot analysis. Northern analysis was performed by standard techniques (38). Immunoblot analysis was performed as previously described (30). Briefly, protein lysates were prepared by lysing cells in modified TNE (50 mM Tris HCl [pH 8.0], 1% Nonidet P-40 [NP-40], 150 mM NaCl, 10 mM NaF, 10 mM $Na_2P_2O_7$, 2 mM EDTA, and 10 μg of phenylmethylsulfonyl fluoride [PMSF], aprotinin, pepstatin, and leupeptin per ml) or, for tissues, EBC lysis buffer (50 mM Tris HCl [pH 7.5], 0.5% NP-40, 150 mM NaCl, and protease inhibitors as described above). Protein (35 μg of cell or 250 μg of tissue lysate) was electrophoresed on sodium dodecyl sulfate (SDS)-7.5 to 12% polyacrylamide gels and transferred to polyvinylidene difluoride membranes. The membranes were stained with Ponceau S (Sigma) to confirm equal loading. The membranes were blocked with 5% skim milk powder in TBST (150 mM NaCl, 2.5 mM KCl, 250 mM Tris base, and 0.05% Tween) and incubated for 1 h at room temperature in primary antibody. Following five washes in TBST, secondary antibody (diluted 1:2,000) was incubated at room temperature for 1 h. After five TBST washes, proteins were visualized by enhanced chemiluminescence detection (Amersham) or Supersignal Ultra (Pierce) for p107 and Rb immunoblots. Primary antibodies used for immunoblotting were anti-cyclin D1 antibody C-20 (Santa Cruz), anti-cyclin E antibody M-20 (Santa Cruz), anti-cyclin A antibody BF683 (Santa Cruz), anti-cyclin B1 antibody GNS1 (Santa Cruz), anti-p130 antibody C-20 (Santa Cruz), anti-p107 antibody C-18 (Santa Cruz), and anti-Rb antibody G3-245 (Pharmingen). Anti-Rb and anti-p107 antibodies were diluted 1:500. All other primary antibodies were diluted 1:1,000.

Growth and cell sort analysis. Primary EF were isolated from 14.5-day postcoitum (dpc) embryos by standard techniques (48). Myoblasts were isolated from 2- to 3-month-old adult mice, purified, and cultured as previously described (40). Cell growth was monitored by plating 5×10^4 EF (WT, $n = 3$; $p107^{-/-}$, $n = 3$) or 10^4 myoblasts (WT, $n = 2$; $p107^{-/-}$, $n = 2$) in 10-cm plates and by counting replicate plates every 20 to 24 h (where n is the number of independently isolated EF or myoblast cultures analyzed).

To determine relative mitotic index, 5×10^4 cells were cultured overnight in 24-well or 35-mm dishes and then incubated with 1 μCi of [^{3}H]thymidine per ml for 2 h. Duplicate plates were rinsed twice with phosphate-buffered saline (PBS), fixed for 30 min at 4°C in 10% trichloroacetic acid (TCA), rinsed with water, and lysed in 200 μl of 0.2 N NaOH, while matched plates or wells were trypsinized to determine cell numbers. TCA-precipitable counts were normalized to cell number. The numbers of independently derived EF cultures analyzed were 6, 6, and 9 for WT, $p107^{+/-}$, and $p107^{-/-}$, respectively. The numbers of independently isolated myoblast cultures analyzed were 2, 2, 2, and 2 for WT, $p107^{-/-}$ (runted), $p107^{-/-}$ (C57BL/6J revertant), and $p107^{-/-}$ (C57BL/6J runted), respectively.

For cell sort analysis, 2×10^4 to 5×10^4 cells were seeded into T25 flasks, and 1 to 2 days later these subconfluent cultures (40 to 60% confluence) were trypsinized, washed twice in PBS, and incubated in PBS containing 50 μg of propidium iodide per ml and 66 U of RNase per ml on ice for 20 to 30 min. Cell cycle analysis was performed with a Becton-Dickinson FACScan flow cytometer. A total of 10^4 cells were analyzed for each sort. Quantitation of cell cycle distribution was performed with MCYCLE software. The numbers of independently derived and analyzed fibroblast cultures were as follows: WT, 5; $p107^{+/-}$, 6; and $p107^{-/-}$, 6. For fluorescence-activated cell sorter (FACS) analysis of the myoblast cultures, two independently derived $p107^{-/-}$ cultures and one WT culture were analyzed.

Cyclin expression and [^{3}H]thymidine incorporation in synchronized EF cells. A total of 5×10^5 WT or 2×10^5 $p107^{-/-}$ cells (to compensate for increased growth rate) were plated at passage 3 and grown to 50 to 60% confluency in 10-cm plates before synchronizing by incubation in 0.1% fetal calf serum (FCS) for 72 h (16). The cells were restimulated to enter the cell cycle with 10% FCS, and protein lysates were prepared every 3 h for 30 h. Three independently derived WT and $p107^{-/-}$ fibroblast cultures were analyzed in duplicate. For [^{3}H]thymidine incorporation assays in synchronized cultures, the cells were treated as described above, and 1 μCi of [^{3}H]thymidine per ml in 10% FCS (or 0.1% for time zero) was added 2 h prior to harvesting triplicate plates at each interval. Counts per minute were normalized to cell numbers (20).

Histopathology and immunohistochemistry. Preparation, fixation, sectioning, and staining of tissue samples for light microscopy of histological preparations were performed by standard techniques (28). Briefly, tissues were fixed in 4% paraformaldehyde in PBS, dehydrated in steps to 70% ethanol, and then stained with Harris' hematoxylin and eosin. Immunohistochemistry was performed on paraformaldehyde-fixed sections with rabbit polyclonal antibody A0398 reactive with myeloperoxidase (Dako).

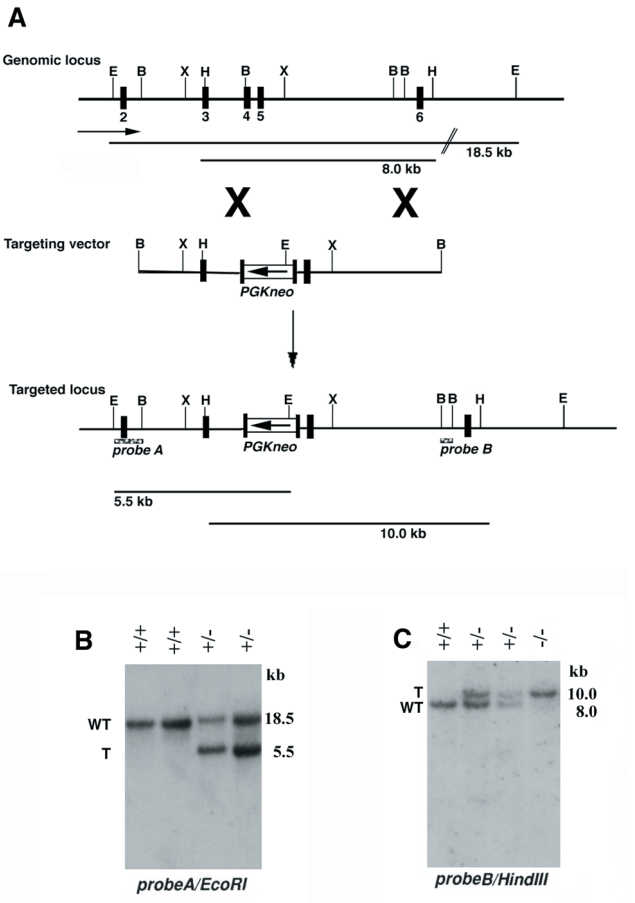

FIG. 1. Targeted disruption of the *p107* gene in ES cells and mice. (A) Structure of the targeting vector, restriction map of the mouse *p107* gene, and structure of the targeted locus following homologous recombination. Exons are depicted as numbered, closed boxes. Genomic fragments (probes A and B) used as probes for Southern blotting are indicated by black boxes. The targeting vector contains PGK-neo in a reverse orientation relative to the *p107* gene. (B and C) Southern blot analysis of genomic DNA isolated from ES cell clones or mouse tails, respectively. The DNA was digested with *Eco*RI and hybridized with probe A or digested with *Hin*dIII and hybridized with probe B. B, *Bam*HI; E, *Eco*RI; RV, *Eco*RV; H, *Hin*dIII; WT, WT allele; T, targeted allele.

RESULTS

Targeted inactivation of *p107* in mice. The *p107* gene was disrupted by homologous recombination in J1 embryonic stem (ES) cells by standard techniques (51). The *p107* targeting vector was constructed by inserting the PGK-neo cassette (39) into exon 4 immediately downstream of the codon encoding aa 165 in the opposite transcriptional orientation (Fig. 1A). Approximately 1% of G418-resistant clones contained the targeted *p107* allele as revealed by Southern analysis (Fig. 1B). Probe A, which was located 5′ of the targeting vector, detected an 18.5-kb *Eco*RI fragment from the WT *p107* allele, whereas a 5.5-kb *Eco*RI fragment was detected following homologous recombination (Fig. 1B). Correct homologous recombination was confirmed by Southern analysis with a probe B located 3′ of the targeting vector and following digestion with additional restriction endonucleases (not shown).

Chimeras were generated following microinjection of two independently derived targeted ES lines into BALB/cJ blasto-

cysts. Southern analysis of tail DNA in germ line progeny revealed the predicted restriction fragment length polymorphism (Fig. 1C). Two independent *p107* mutant mouse lines were derived into the germ line, and, since the observed homozygous phenotype was completely identical in all experiments, these are hereafter discussed together. Interbreeding of heterozygous *p107* mice yielded an approximate Mendelian ratio of 1:2:1 between WT, heterozygous mutant, and homozygous mutant mice, respectively. As summarized in Table 2, the genotypes of the first 265 mice were 71 WT mice (26.8%), 136 $p107^{+/-}$ mice (51.3%), and 58 $p107^{-/-}$ mice (21.9%). Therefore, the absence of p107 appeared not to significantly affect embryonic development or postnatal survival. However, $p107^{-/-}$ mice did exhibit a profound difference in growth rate in the immediate postnatal period as described below.

To confirm that the engineered disruption of exon 4 in *p107* by PGK-neo had generated a null mutation, we performed Northern and immunoblot analyses with RNA and protein isolated from E14.5 embryos. Northern analysis was performed on poly(A)$^+$ mRNA isolated from EF with various probes. As shown in Fig. 2A, with the full-length mouse *p107* cDNA as a probe, the mature 4.8-kb *p107* mRNA was readily detected in RNA isolated from WT EF. However, $p107^{+/-}$ EF expressed a second RNA about 300 nucleotides smaller than the full-length *p107* mRNA, and $p107^{-/-}$ EF expressed only the smaller RNA (Fig. 2A, compare lanes 1, 2, and 3). The truncated RNA did not hybridize a neo probe (not shown). Nuclease S1 analysis with cDNA probes from either side of the integration site revealed that the truncated *p107* transcript originates from the disrupted exon as a sense transcript (not shown). Therefore, we surmise that the truncated RNA expressed from the mutant *p107* allele is initiated from the PGK-1 promoter, but in the direction opposite to that for the normal PGK-1 transcriptional initiation, to generate a truncated sense *p107* transcript. A similar phenomenon has been previously reported for mice carrying a targeted MyoD null mutation (51).

Immunoblot analysis was performed with antiserum C18 reactive with the carboxyl-terminal 18 aa of p107. The p107 protein was readily detected in extracts from 14.5-dpc WT embryos, and reduced levels were observed in extracts from 14.5-dpc $p107^{+/-}$ embryos (Fig. 2B, lanes 1 and 2). No detectable product was observed in lysates derived from $p107^{-/-}$ embryos (Fig. 2B, lane 3). Moreover, no smaller-molecular-weight species were apparent in extracts prepared from mutant embryos. Therefore, we conclude that disruption of *p107* exon 4 with PGK-neo generated a null allele.

Immunoblot analysis was also performed with antiserum C20 reactive with p130 and with antiserum G3-245 reactive with Rb. The levels of p130 were similar in extracts prepared from WT, $p107^{+/-}$, and $p107^{-/-}$ embryos (Fig. 2C; compare lanes 1, 2, and 3). By contrast, Rb levels were reproducibly increased by about twofold in extracts prepared from $p107^{-/-}$ embryos ($n = 5$) and were unaltered in extracts prepared from $p107^{+/-}$ embryos (Fig. 2D; compare lanes 1, 2, and 3). Therefore, our data raise the possibility that p107 indirectly or directly negatively regulates *Rb* expression.

Fibroblasts and myoblasts lacking *p107* display accelerated cell cycle kinetics. To facilitate the characterization of cell cycle kinetics of cells lacking *p107*, we derived primary cultures of WT, $p107^{+/-}$, and $p107^{-/-}$ EF from 14.5-dpc sibling embryos following timed matings of heterozygous mutant mice. Notably, $p107^{-/-}$ embryos at 14.5 dpc were indistinguishable from littermates. Cell growth was monitored by counting the increase in the number of early-passage viable EF in subconfluent replicate cultures over 2 weeks. We observed the doubling time of WT EF derived from 14.5-dpc embryos to be about twofold slower than that in EF derived from 12.5-dpc embryos. WT and $p107^{+/-}$ EF derived from 14.5-dpc embryos doubled in number about every 60 h (Fig. 3A). A 60-h doubling time is typical for WT EF cultures derived from embryos after 13.5 dpc (16). In contrast, $p107^{-/-}$ EF cultures displayed a markedly increased growth and doubled in number about every 35 h (Fig. 3A). Moreover, $p107^{-/-}$ EF incorporated twofold more [^{3}H]thymidine per hour than WT and $p107^{+/-}$ EF ($n = 5$) (Fig. 3C).

The growth rate of early-passage primary myoblasts isolated from adult mice was characterized to examine whether the acceleration in cell cycle kinetics was also present in adult somatic cell cultures. WT myoblasts doubled in number about every 42 h, whereas $p107^{-/-}$ myoblasts doubled in number

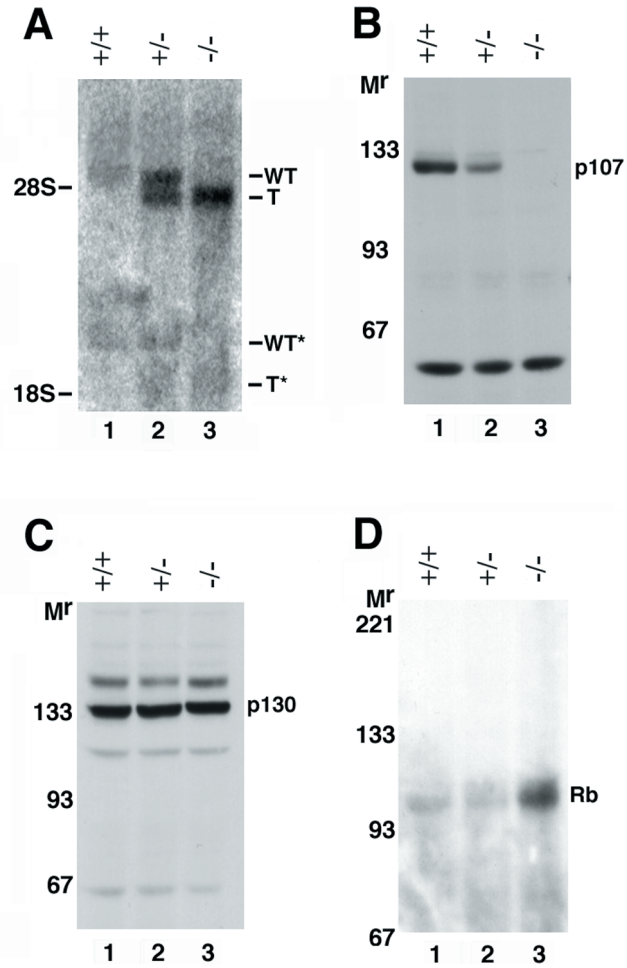

FIG. 2. Expression of Rb family members in *p107*-deficient mice. (A) Northern analysis of poly(A)-selected RNA prepared from WT, $p107^{+/-}$, and $p107^{-/-}$ EF subconfluent cultures with the full-length mouse *p107* cDNA as a probe. The targeted allele (T) gave rise to a truncated sense transcript that likely originated from within the PGK-1 promoter. The alternatively spliced 2.4-kb *p107* transcript (*) was also detected (29). (B) Immunoblot analysis with anti-p107 polyclonal antibody revealed no detectable p107 protein or truncated version of the protein in extracts prepared from $p107^{-/-}$ 14.5-dpc embryos. (C) Immunoblot analysis with anti-p130 polyclonal antibody revealed approximately similar levels of p130 in extracts prepared from WT, $p107^{+/-}$, and $p107^{-/-}$ 14.5-dpc embryos. (D) Immunoblot analysis with anti-Rb polyclonal antibody revealed an approximately twofold increase in levels of Rb in extracts prepared from $p107^{-/-}$ 13.5-dpc embryos, relative to extracts prepared from WT and $p107^{+/-}$ siblings. WT, WT *p107* transcript; T, truncated *p107* transcript; M^r, apparent relative mobility (in kilodaltons).

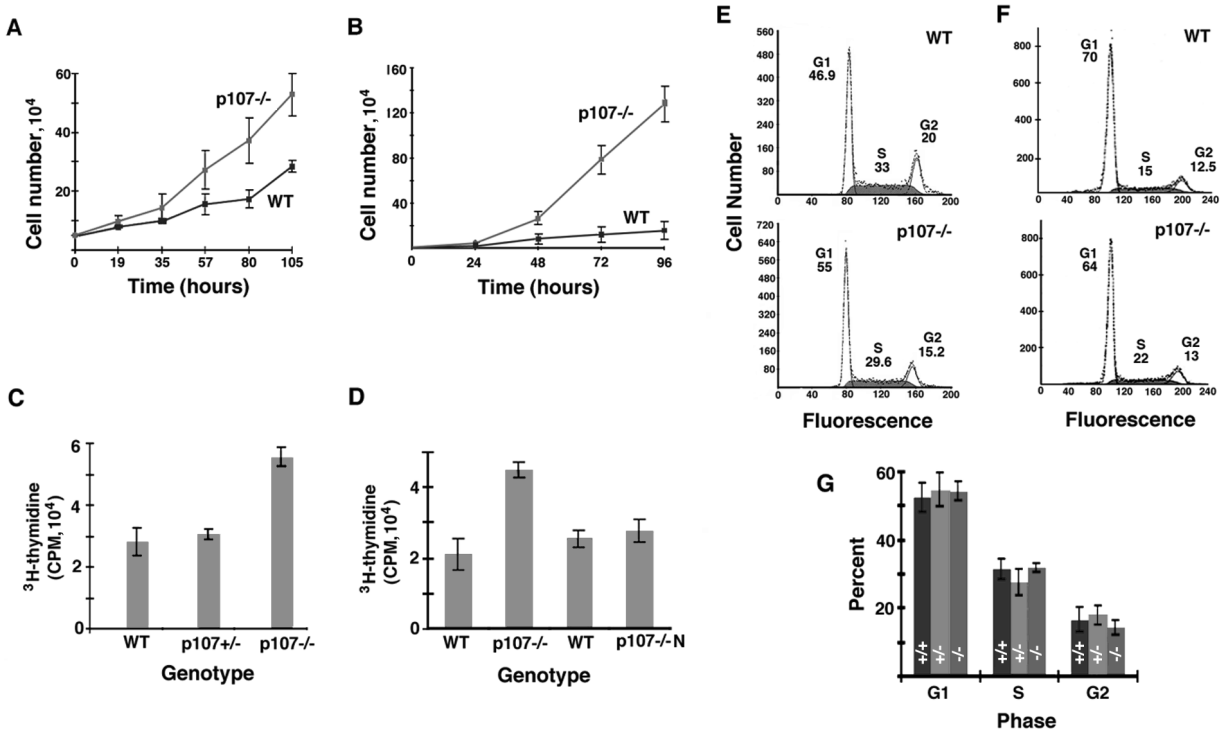

FIG. 3. Twofold acceleration in cell cycle kinetics in $p107^{-/-}$ fibroblasts and myoblasts. (A) Growth curve for cultured WT and $p107^{-/-}$ EF isolated from 14.5-dpc embryos ($n = 3$). Heterozygous EF displayed the same growth kinetics as WT EF (not shown). (B) Growth curve for cultured WT and $p107^{-/-}$ primary myoblasts isolated from adult mice ($n = 2$). (C) Growth rates of WT, $p107^{+/-}$, and $p107^{-/-}$ EF as revealed by [^{3}H]thymidine incorporation following 2 h of exposure in exponential growth ($n = 5$). (D) Growth rates of WT myoblasts ($n = 2$) and myoblasts isolated from a $p107^{-/-}$ mouse of normal size ($n = 3$) versus myoblasts isolated from runted $p107^{-/-}$ littermates ($n = 2$), derived following a backcross to C57BL/6J mice (see Table 2), as revealed by [^{3}H]thymidine incorporation following 2 h of exposure in exponential growth. (E) Example of flow cytometry of EF cultures in exponential growth indicated that the proportion of mutant EF in the different phases of the cell cycle is similar to that for the WT. (F) Example of flow cytometry of primary myoblast cultures in exponential growth indicated that the proportion of mutant cells in the S phase is increased by about 7% compared to WT. However, this shift from G_1 to S can be accounted for by a decrease in the rate of spontaneous differentiation in growth medium from 12% in WT to 1.5% in the mutant. (G) Flow cytometry of EF cultures in exponential growth indicated that the proportions of mutant EF ($n = 6$) in G_1, S, and G_2 were similar to those for WT ($n = 4$) and $p107^{+/-}$ ($n = 6$) fibroblasts. Errors are expressed as standard deviations where n is the number of independently derived cell cultures analyzed.

about every 17 h ($n = 2$) (Fig. 3B). Similarly to EF, $p107^{-/-}$ myoblasts incorporated twofold more [^{3}H]thymidine per hour than WT myoblasts ($n = 2$) (Fig. 3D). Therefore, we conclude that the observed acceleration in cell cycle kinetics was not limited to EF.

Flow cytometry of independently isolated EF cultures ($n = 6$) in exponential growth indicated that the proportion of cells in G_1, S, and G_2 was unaltered in the absence of p107. The proportion of WT and mutant EF cells in G_1 was about 54%, the proportion in S was about 30%, and the proportion in G_2 was about 16% (Fig. 3E and G). However, analysis of forward versus side scatter during the flow cytometry indicated no significant difference in cell size between $p107^{-/-}$ and WT EF (not shown). Flow cytometry of primary myoblast cultures indicated a decrease of approximately 6% in the proportion of cells in G_1 and an increase of approximately 7% in the proportion of cells in S phase in the two cultures analyzed (Fig. 3F). Importantly, this shift from G_1 to S can be accounted for by an observed eightfold decrease in the rate of spontaneous differentiation in growth medium from 12% in the WT to 1.5% in the mutant as assessed with antibody MF20 reactive with myosin heavy chain (data not shown). Importantly, both WT and $p107^{-/-}$ EF cultures exhibited similarly nil rates of apoptosis, as judged by terminal-transferase-mediated dUTP-biotin nick end labeling (TUNEL) analysis, annexin V histochemistry (not shown), and the absence of significant numbers of sub-G_1 cells detected by cell sort analysis (Fig. 3E). In addition, continuous labelling of EF cultures with BrdU for 30 and 60 h revealed no significant difference in the proportion of unstained noncycling cells between populations (not shown). Taken together, these data indicate that the lengths of the different phases of the cell cycle were proportionately reduced by a factor of approximately 2 in both EF and myoblasts lacking *p107*.

The absence of *p107* in EF clearly resulted in an acceleration of approximately twofold in cell cycle kinetics. To investigate the consequence of these altered cell cycle kinetics for cyclin expression, we performed immunoblot analysis with a panel of antibodies reactive with cyclins D1, E, A, and B1 on extracts isolated from synchronized cultures of EF. Western analysis was performed for three independently isolated EF cultures of each genotype, all in duplicate. Cultures were serum starved to arrest cells in G_0 and then stimulated with serum to initiate entry into the cell cycle. Consistent with an acceleration in cell cycle kinetics, we observed correspondingly more rapid transit through S phase in serum-stimulated $p107^{-/-}$ fibroblasts as determined by [^{3}H]thymidine incorporation (Fig. 4I), although the transit from the G_0 phase to S was only slightly attenuated. These data indicated that the loss of *p107* did not apparently accelerate entry into the G_1 phase from an arrested state.

As shown in Fig. 4, cyclin D1 and cyclin E were upregulated in synchronized WT EF about 12 h after serum stimulation (Fig. 4A and C). Cyclin A was upregulated about 18 h after stimulation, and cyclin B1 was upregulated about 24 h after

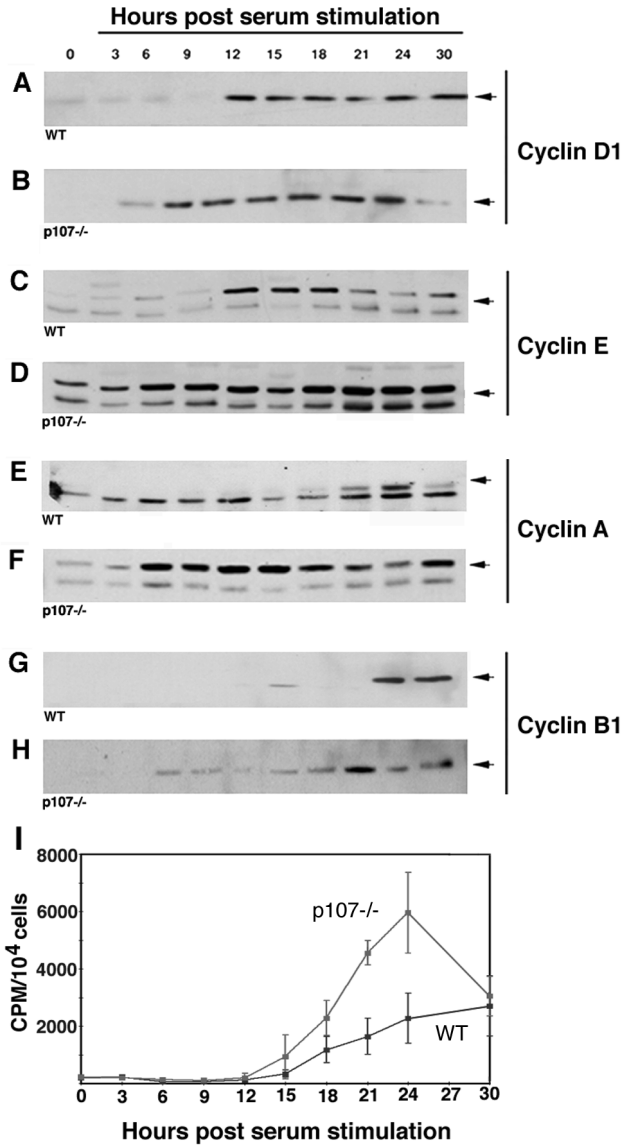

FIG. 4. (A through H) Immunoblot analysis of G_1 cyclin expression in $p107^{-/-}$ fibroblasts. Protein lysates were prepared at the indicated times after readdition of serum to EF synchronized by serum starvation ($n = 3$). Cyclin proteins were detected by polyclonal (cyclins D1, E, and A) or monoclonal (cyclin B1) antibodies. Note the disregulation in induction of cyclin expression in $p107^{-/-}$ cells with constitutively expressed cyclin E and cyclins A and B1 expressed about 12 and 18 h earlier, respectively, than normal. (I) Incorporation of [^{3}H]thymidine at intervals following serum stimulation indicated that $p107^{-/-}$ EF reproducibly transit S phase faster than WT. n = the number of independently derived cultures, each of which was characterized twice by Western analysis.

stimulation (Fig. 4E and G). In contrast, $p107^{-/-}$ EF displayed constitutive high-level expression of cyclin E that continued to increase throughout the time interval investigated (Fig. 4D). In addition, cyclins A and D1 were upregulated about 6 h following stimulation (Fig. 4B and F). Lastly, cyclin B1 was upregulated about 6 h following stimulation of the mutant EF cells (Fig. 4H). In summary, during the synchronized progression of mutant EF cells from G_0 through S phase, cyclin E was constitutively expressed, cyclin D1 was expressed about 6 h earlier than normal, cyclin A was expressed about 12 h earlier than normal, and cyclin B1 was expressed about 18 h earlier than normal. Interestingly, constitutive expression of cyclin E is also observed in Rb-deficient EF, although the doubling time was unaltered (20). Taken together, these data indicate that p107 is required for the appropriate regulation of cyclin expression and plays an important role in regulating the overall length of the cell cycle, but in a strain-dependent manner.

TABLE 1. Reduced growth of *p107*-deficient mice[a]

Mouse	Wt (g)	Sample size (n)
Male		
WT	12.4 ± 1.5	18
$p107^{+/-}$	12.1 ± 0.81	16
$p107^{-/-}$	6.5 ± 0.6	14
Female		
WT	10.8 ± 1.6	15
$p107^{+/-}$	10.4 ± 0.71	16
$p107^{-/-}$	4.5 ± 1.3	12

[a] Offspring from F_1 $p107^{+/-}$ × F_1 $p107^{+/-}$ breedings were weighed at 21 days postpartum. Male $p107^{-/-}$ mice were 52% of their normal weight, whereas female $p107^{-/-}$ mice were 42% of their normal weight. Errors are expressed as standard deviations.

Severe postnatal growth deficiency in $p107^{-/-}$ mice. Mutant embryos at 14.5 dpc and newborn pups were indistinguishable from their siblings in both size and morphology (not shown). Strikingly, by 3 weeks of age, $p107^{-/-}$ pups were uniformly about half the normal weight of their heterozygous and WT littermates (Table 1; compare Fig. 5A and B). However, by 12 weeks of age, $p107^{-/-}$ mice reached about 80% the weight of heterozygous and WT animals. In addition, adult mutant animals of as much as 15 months of age displayed a normal physical appearance and exhibited no notable abnormal behavioral traits. Histological inspection of organs throughout the $p107^{-/-}$ mice revealed no apparent anatomical abnormalities. Moreover, TUNEL analysis revealed no abnormal increase in numbers of apoptotic cells.

To examine the growth kinetics of $p107^{-/-}$ mice, animals were weighed at regular intervals for 60 days following birth (Fig. 5C and D). These data suggested that newborn $p107^{-/-}$ pups failed to grow at the same rate as their WT and heterozygous littermates in the immediate postnatal period. However, mutant mice were weaned at 4 weeks postpartum and reached sexual maturity at the normal time (6 weeks for females and 8 weeks for males). Taken together, these data suggest that mice deficient in *p107* are not delayed in postnatal development but instead exhibit a reduced rate of postnatal growth.

Newborn mutant pups exhibited normal suckling behavior, with milk evident in their stomachs within a few hours after birth. In 3-week-old pups, histological examination of the pancreas revealed a normal appearance, with an absence of zymogen particles, indicating that *p107* mutant animals were likely absorbing nutrients in a normal manner. However, consistent with the reduced overall size of the mutant animals and smaller organs, we observed a reduced cellularity in many tissues, i.e., the retina, gut epithelium, skin, pancreas, spleen, and thymus, etc. (data not shown).

The normal birth size and reduced postnatal growth of newborn animals lacking *p107* suggested that this phenotype was due to hormonal deficiencies. However, serum levels of growth hormone appeared to be completely normal in 4-week-old $p107^{-/-}$ mice. Moreover, Northern analysis of total RNA isolated from $p107^{-/-}$ tissues revealed normal levels of IGF-1

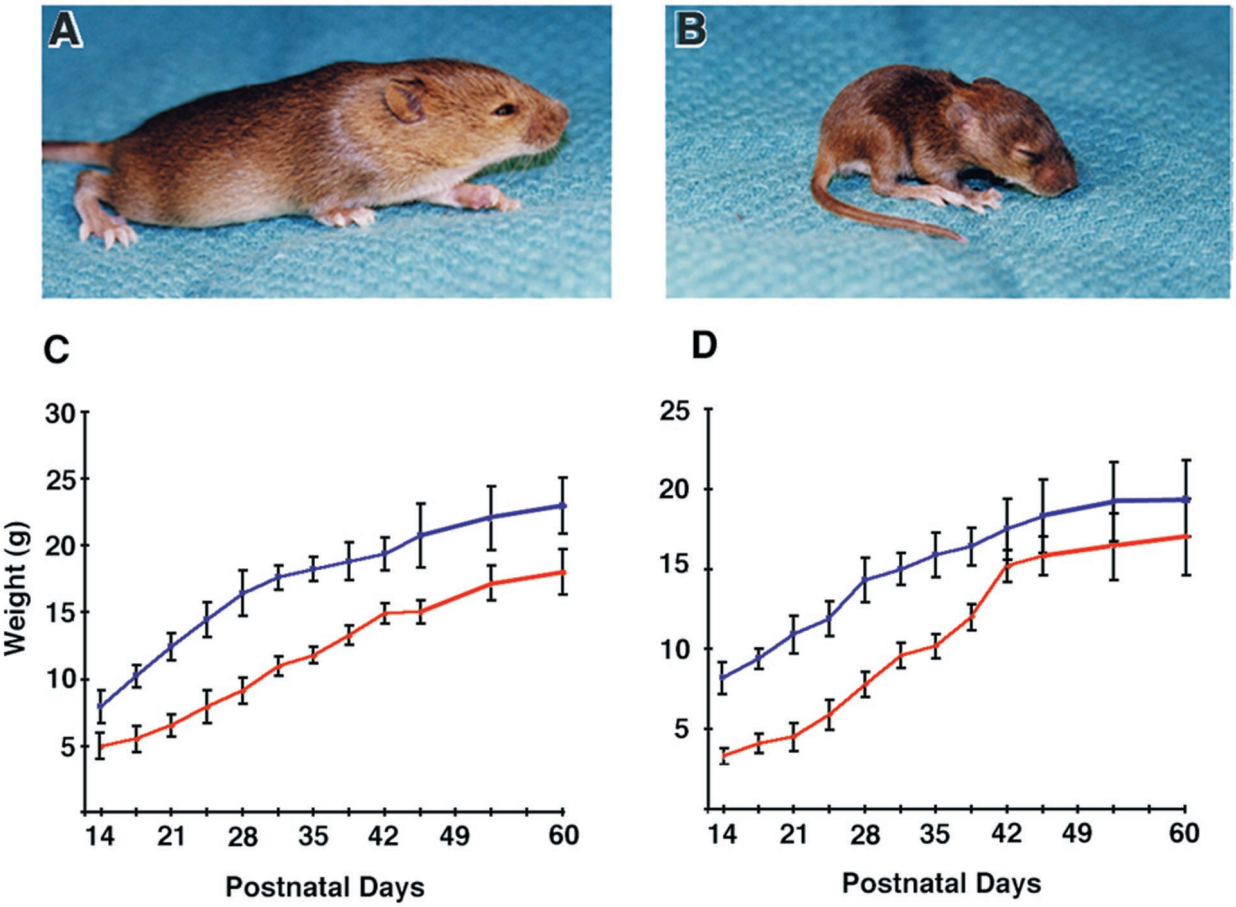

FIG. 5. Severe postnatal growth deficiency in $p107^{-/-}$ mice. WT (A) and *p107*-deficient (B) littermates at 12 days of age derived from an F_1 $p107^{+/-} \times$ F1 $p107^{+/-}$ cross. Note the severe postnatal growth deficiency evident in $p107^{-/-}$ pups (see Table 1). (C) Growth curve of male WT ($n = 7$) (blue) and $p107^{-/-}$ ($n = 7$) (red) mice derived from heterozygous mutant matings. Male mice lacking *p107* by 21 days of age were about 52% of their normal weight. (D) Growth curve of female $p107^{+/-}$ ($n = 9$) (blue) and $p107^{-/-}$ ($n = 8$) (red) mice derived from heterozygous mutant matings. Female mice by 21 days of age were about 42% of their normal weight. Errors are expressed as standard deviations.

mRNA. Therefore, the basis of the reduced postnatal growth of *p107*-deficient mice remains unclear.

Diathetic myeloid proliferative disorder in $p107^{-/-}$ mice. All animals were housed in a barrier facility, with rigorous screening procedures in place to ensure a substantially pathogen-free environment. Nevertheless, we observed a high incidence of morbidity in mice lacking *p107*, often in young mice between 2 and 4 months of age. Approximately 10% of $p107^{-/-}$ mice suffered unexpected death or displayed symptoms suggestive of opportunistic infections of a severity that warranted euthanasia. Histological analyses of these animals revealed the presence of an inflammatory response suggestive of acute lung and intestinal infections. Histological analysis of lung, gut, and skin of unselected $p107^{-/-}$ mice at 10 months of age ($n = 9$) revealed that 70% exhibited evidence of either acute or chronic inflammation, with tissues containing extensive infiltration of either neutrophils or of macrophages, plasma cells, and mast cells. In some of these $p107^{-/-}$ animals, the inflammation was manifested as skin ulcers and abscesses. Importantly, no infections, sudden death, or histological evidence of inflammation was observed in WT or $p107^{+/-}$ mice. Taken together, these data suggested that the immune response of $p107^{-/-}$ mice was compromised.

Further histological analysis of $p107^{-/-}$ mice revealed a high proportion of animals that displayed a pattern of changes consistent with the presence of a myeloproliferative disorder. In the marrow of the sternum, we observed a hypercellularity, with a strong shift to myeloid lineages (compare Fig. 6A and B). Examination of spleens revealed extensive extramedullary hematopoiesis (EMH) within the red pulp that was predominantly myeloid in composition (compare Fig. 6C and D). However, the most striking change was the presence of EMH in liver, consisting mostly of well-developed islands, many of which were located in the walls of blood vessels (Fig. 6E and F). The EMH in the spleen and liver was almost completely myeloid in composition, as confirmed by cytomorphology and immunohistochemistry with antibody reactive with myeloperoxidase (Fig. 7A and B).

Myeloid cell progenitors (CFU of granulocyte-macrophages [CFU-GM]) were enumerated following culture of marrow isolated from the femurs from 5-week-old mice. Importantly, we observed significantly increased numbers of myeloid progenitors in the femurs of two of three $p107^{-/-}$ mice. The numbers of CFU-GM in the two elevated $p107^{-/-}$ samples were increased by 2.7-fold ($P = 0.002$) and 12-fold ($P < 0.0001$) relative to three WT sibling mice. Sites of predominantly myeloid EMH were also noted in the thymus, pancreas, kidneys, and skeletal muscles of some mutant animals, as detected with anti-myeloperoxidase antibody (Fig. 7). In affected mutant animals, the lymph nodes from the pulmonary hilus

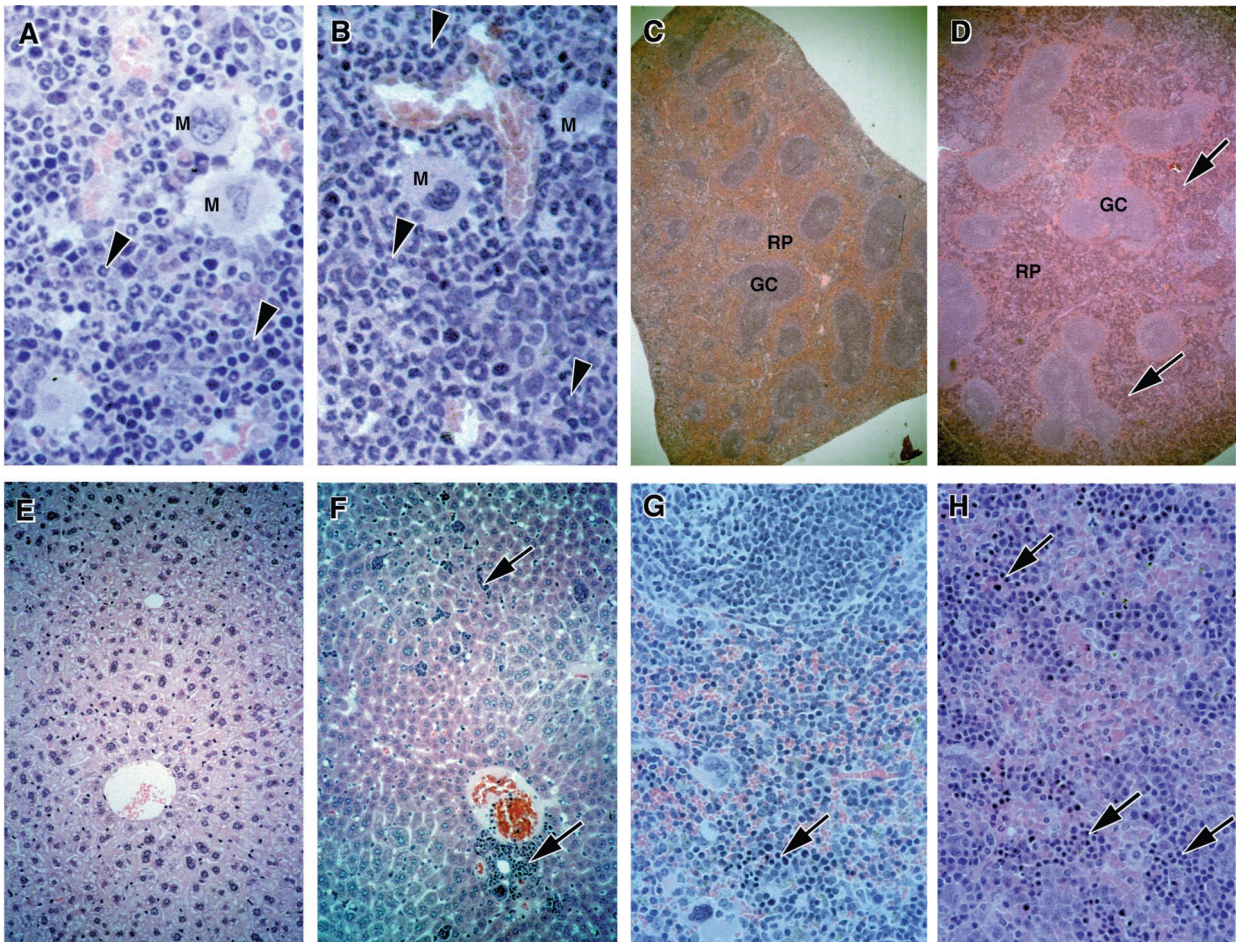

FIG. 6. Myeloproliferative disorder in $p107^{-/-}$ mice. Histological analysis of hematoxylin-and-eosin-stained sections revealed a hypercellularity with a strong shift to myeloid lineages in the marrow of $p107^{-/-}$ mice (B) relative to WT mice (A). Examination of mutant spleens (D and H) revealed extensive extramedullary hematopoiesis within the red pulp that was predominantly myeloid in composition. Normal spleen from a WT littermate (C and G) was also examined. A high proportion of $p107^{-/-}$ livers contained extensive infiltration of well-developed hematopoietic islands that were also mostly myeloid in composition (F). Normal liver from a WT littermate (E) was also examined. Immunohistochemistry with antimyeloperoxidase antibody was used to confirm the myeloid identities of cells in the liver, spleen, and marrow (see Fig. 7A through C). Samples shown are from 12-month-old mice. Arrowheads, myeloid cells; arrows, sites of myeloid metaplasia in the spleen and liver. M, megakaryocyte; RP, red pulp; GC, germinal centers. Magnifications were ×400 (A and B), ×150 (C and D), and ×200 (E, F, G, and H).

were found to be unaltered and the marrow and sites of EMH had not undergone fibrosis, as revealed by reticulin staining. Moreover, the proportion of blast cells relative to their differentiated derivatives appeared normal. Therefore, the disorder resembles a hyperplasia of the myeloid compartment rather than an overt neoplasia.

The proportion of the mutant animals that displayed the disorder appeared to increase with the age of the animal. Between 2 and 6 months of age, $p107^{-/-}$ mice ($n = 8$) often exhibited evidence of metaplastic myeloid proliferation in the spleen but not in the liver. However, 54% of $p107^{-/-}$ mice over 6 months of age ($n = 13$) exhibited overt myeloid metaplasia in the liver and spleen, ranging from medium to severe. By contrast, only a small number of well-dispersed individual myeloid cells were detected by immunohistochemistry with myeloperoxidase antibody in sections of liver in 1 of 10 WT animals and in one of eight $p107^{+/-}$ animals (not shown). Importantly, no hyperplastic or neoplastic changes were noted in a histological survey of a variety of other tissues from mutant mice. Taken together, these data indicate that $p107^{-/-}$ mice develop a diathetic myeloproliferative disorder that possibly predisposes the animals to opportunistic infections.

The *p107* mutant phenotype is strain dependent. The relatively normal phenotype of the $p107^{-/-}$ mice previously generated in a mixed 129/Sv:C57BL/6J genetic background (32) and the marked phenotype of $p107^{-/-}$ mice crossed into a BALB/cJ background suggested that the penetrance of the *p107* mutant phenotype was dependent on the mouse strain genetic background. To test this hypothesis, we bred male and female F_1 $p107^{+/-}$ mice that were progeny of the founding chimeras and BALB/cJ mice with either C57BL/6J or BALB/cJ mice. The resulting B1 $p107^{+/-}$ mice were then interbred to generate $p107^{-/-}$ mice. Importantly, the B1 $p107^{+/-}$ mice derived from the F_1 $p107^{+/-}$ × C57BL/6J cross had one set of C57BL/6J chromosomes and a second set composed of an undefined mixture of BALB/cJ and 129/Sv chromosomes. The B1 $p107^{+/-}$ mice derived from the F_1 $p107^{+/-}$ × BALB/cJ cross had one set of BALB/cJ chromosomes and a second set composed of an undefined mixture of BALB/cJ and 129/Sv chromosomes. Therefore, the interbreeding of B1 $p107^{+/-}$ mice derived from such backcrosses allows an assessment of the contribution of BALB/cJ and C57BL/6J genetic backgrounds to the penetrance of the phenotype.

As described above, $p107^{-/-}$ animals derived from an F_1 ×

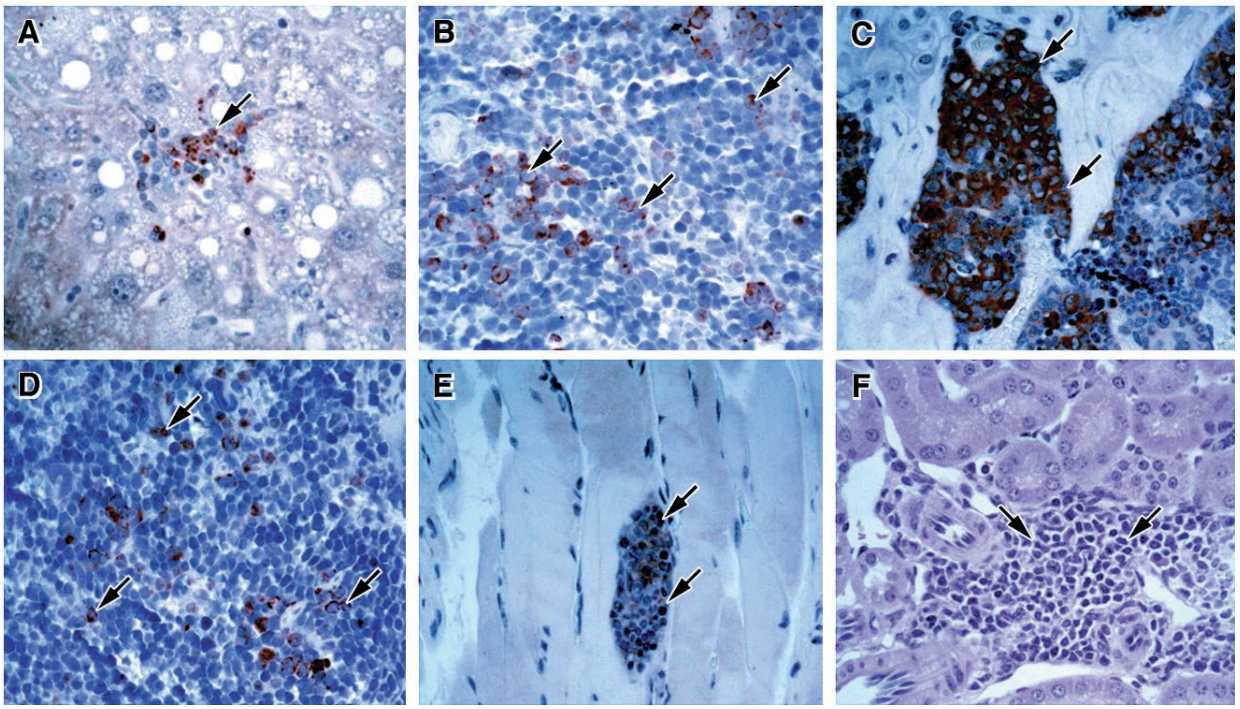

FIG. 7. Unusual sites of myeloproliferation in $p107^{-/-}$ mice. Myeloid cells were detected by immunostaining with antibody reactive to myeloperoxidase in liver (A), spleen (B), marrow (C), thymus (D), and skeletal muscle (E). Myeloid EMH was also detected in the kidneys of some $p107^{-/-}$ animals (F). Samples shown are from 12-month-old mice. Magnification, ×400.

F_1 mating displayed 100% penetrance of the growth phenotype (Table 2). In a small proportion of F_2 $p107^{-/-}$ × F2 $p107^{-/-}$ matings, we observed litters that contained a mixture of runted and normal-sized F_3 $p107^{-/-}$ mice, suggesting that multiple recessive second-site modifier genes were segregating in the population. Interbreeding of B1 $p107^{+/-}$ mice derived from a F_1 $p107^{+/-}$ × BALB/cJ mating gave rise to $p107^{-/-}$ mice that also exhibited a 100% penetrance of the growth phenotype, indicating that a background enriched for BALB/cJ was permissive for penetrance (Table 2). Additionally, $p107^{-/-}$ mice were only 35% of the size of heterozygous or WT littermates at 3 weeks of age, indicating that the growth phenotype was more severe in a genetic background enriched for BALB/c. In contrast, interbreeding of B1 $p107^{+/-}$ mice derived from a F_1 $p107^{+/-}$ × C57BL/6J mating gave rise to a high proportion of $p107^{-/-}$ mice that exhibited no growth deficit, indicating that a background enriched for C57BL/6J suppressed the phenotype (Table 2). Importantly, $p107^{-/-}$ mice segregated discretely into two weight groups at 3 weeks of age, suggesting that the trait was not quantitative in nature (Table 1). Moreover, while primary myoblasts derived from runted $p107^{-/-}$ mice displayed a twofold acceleration in cell cycle kinetics, primary myoblasts isolated from normal-sized $p107^{-/-}$ mice exhibited normal cell cycle kinetics (Fig. 3D). In addition, the reduced number of viable $p107^{-/-}$ offspring in mice derived from the BALB/cJ backcross supports the assertion that the severity of the $p107^{-/-}$ phenotype is increased in a genetic background enriched for BALB/cJ. Taken together, these data support the existence of multiple second-site modifier genes that have a potentially epistatic relationship with *p107*.

DISCUSSION

We have generated a null allele of *p107* by gene targeting in mice and crossed the mutant allele into BALB/cJ and C57BL/6J strains of mice. Mice lacking *p107* crossed into a BALB/cJ genetic background exhibited a marked deficiency in postnatal growth but were viable and fertile. By 1 year of age, over half of the mutant mice developed a severe myeloproliferative disorder characterized by myeloid hyperplasia in the marrow and myeloid metaplasia in the spleen and liver. Embryonic fibroblasts derived from the mutant animals displayed a markedly increased growth rate associated with constitutive expression of cyclin E. Importantly, following a backcross to C57BL/6J mice, $p107^{-/-}$ animals were derived that were phenotypically normal. These data clearly indicate that p107 plays a central role in regulating the cell cycle, but in a strain-dependent manner.

Hurford et al. performed a careful analysis of several E2F-

TABLE 2. Genetic background specifies the penetrance of the $p107^{-/-}$ phenotype

Genotype	Value with the following intercrosses:		
	Chimera × BALB/cJ ↓ $F_1^{+/-}$ × $F_1^{+/-}$ [a]	$F_1^{+/-}$ × BALB/cJ ↓ $B1^{+/-}$ × $B1^{+/-}$ [b]	$F_1^{+/-}$ × C57BL/6J ↓ $B1^{+/-}$ × $B1^{+/-}$ [c]
$WT^{+/+}$	71	49	74
$p107^{+/-}$	136	104	137
Runted $p107^{-/-}$	58	25	9
Normal $p107^{-/-}$	0	0	29

[a] The F_1 $p107^{+/-}$ progeny of the founding chimeras bred with BALB/cJ mice were interbred to yield $p107^{-/-}$ mice that uniformly displayed the runted growth phenotype.

[b] The B1 $p107^{+/-}$ mice derived from an F_1 $p107^{+/-}$ × BALB/cJ mating were interbred to produce $p107^{-/-}$ mice that also exhibited a 100% penetrance of a more severe runted growth phenotype.

[c] The B1 $p107^{+/-}$ mice derived from an F_1 $p107^{+/-}$× C57BL/6J mating were interbred to generate litters that contained both normal and runted $p107^{-/-}$ mice.

responsive genes in EF isolated from mice carrying mutations in different *Rb* family genes (24). No change in E2F-regulated genes was observed in fibroblasts lacking either *p107* or *p130*. However, $Rb^{-/-}$ and $p107^{-/-}$:$p130^{-/-}$ fibroblasts exhibited disregulation of distinct E2F-regulated genes. Cyclin E and p107 were derepressed in $Rb^{-/-}$ fibroblasts during the G_1-S transition, whereas B-myb, cdc2, E2F1, thymidylate synthase, ribonucleotide reductase M2, cyclin A2, and DHFR were derepressed in $p107^{-/-}$:$p130^{-/-}$ fibroblasts during the G_0-G_1 transition. Moreover, cell cycle kinetics and Rb expression were unaltered in $p107^{-/-}$:$p130^{-/-}$ fibroblasts (24). In contrast, in $p107^{-/-}$ fibroblasts in a genetic background enriched for BALB/cJ, we observed a twofold shortening in the cell cycle duration, constitutive expression of cyclin E, premature expression of cyclins A, D1, and B1, and upregulation of Rb. Therefore, in a genetic background enriched for BALB/cJ, p130 and Rb cannot fully substitute for the absence of p107.

Our data are consistent with the idea that p107 is a key player in mediating negative control of the E2F family of transcription factors. Clearly, forced expression of heterodimerized E2F family members is sufficient to induce expression of E2F-regulated genes (43, 57) and to drive growth-arrested cells into S phase (15, 27, 35, 47, 54). In addition, the cyclin E promoter contains E2F binding sites that confer cell cycle-regulated expression (7, 17, 44). Moreover, the cyclin A promoter is believed to be negatively regulated by p107, since it contains an E2F site that binds a complex containing E2F/p107 that is disrupted through interaction with cyclin E/cdk2 (23, 52, 64). These data support the hypothesis that p107 functions as a key negative regulator acting to attenuate cellular proliferation. Our data also suggest that p107 may have a more extensive role than that previously believed in regulating the expression of G_1 cyclins.

In the immediate postnatal period, *p107*-deficient pups displayed a markedly reduced growth rate, leading to a runted appearance. Because newborn $p107^{-/-}$ pups and E14 embryos were unaltered in size from their WT and heterozygous siblings, we considered the hypothesis that the reduced postnatal growth reflected a hormonal deficiency. Candidate hormones involved in stimulating postnatal growth include growth hormone (GH) and insulin-like growth factor 1 (IGF-1) (2, 45). However, serum analysis revealed normal levels of GH in $p107^{-/-}$ mice, and Northern analysis of tissue IGF-1 levels revealed no difference in mRNA levels. In addition, because $p107^{-/-}$ mice reached sexual maturity at the normal time and displayed normal fecundity and lactation, we believe that pituitary function was normal in mutant mice.

Interestingly, transgenic mice overexpressing Rb display a runted appearance and altered growth kinetics reminiscent of that observed in $p107^{-/-}$ mice (5). Importantly, we observed an approximately twofold increase in Rb levels in $p107^{-/-}$ embryos in an enriched BALB/cJ genetic background (Fig. 2D), whereas no change in Rb levels was detected in $p107^{-/-}$ embryos in a mixed 129/Sv:C57BL6/J genetic background (24). Therefore, it is interesting to speculate that the reduced growth of $p107^{-/-}$ mice is simply a consequence of the upregulation of Rb that appears to occur specifically in a BALB/cJ genetic background. To assess whether the $p107^{-/-}$ postnatal growth phenotype was a consequence of the elevated Rb levels, matings to generate $p107^{-/-}$:$Rb^{+/-}$ mice were performed. However, in contrast to the viable phenotype of $p107^{-/-}$:$Rb^{+/-}$ mice in a mixed 129/Sv:C57BL6/J genetic background (32), $p107^{+/-}$:$Rb^{+/-}$ mice in a background enriched for BALB/cJ died in utero between 12.5 and 14.5 dpc (29a). Therefore, because two alleles of Rb are required for the viability of $p107^{-/-}$ mice in a genetic background enriched for BALB/cJ, we were unable to genetically determine whether upregulation of Rb influences growth rate.

Mice lacking *p107* exhibited a diathetic myeloproliferative disorder characterized by myeloid hyperplasia in the marrow and myeloid metaplasia in the spleen and liver. The penetrance of the myeloproliferative disorder increased with the age of the animals, suggesting that secondary events were required for progression of the disease. The secondary events leading to a myeloproliferative disorder could be either mutations in other genes, for example, activating mutations in oncogenes resulting in clonal hyperplasia, or, alternatively, conditions leading to constitutive stimulation of the myeloid lineage, for example, recurring opportunistic infections leading to polyclonal hyperplasia.

The molecular basis for the myeloproliferative disorder in $p107^{-/-}$ mice remains to be resolved; however, we favor the hypothesis that recurring opportunistic infections lead to development of a polyclonal myeloid hyperplasia. Several possibilities can be considered. For example, in myeloid cells, p107 appears to be required for tumor growth factor (TGF) β1 inhibition of interleukin-3 (IL-3)-dependent growth via suppression of c-Myc activity (3). In addition, p107 is believed to negatively regulate c-Myc activity via specific interactions with the c-Myc amino-terminal transcriptional activation domain (4). Mutations in the amino-terminal portion of Myc in lymphoma patients abrogate interactions with p107, leading to inappropriately increased c-Myc activity (19, 22). Lastly, the P2 promoter of c-Myc contains an E2F site that is negatively regulated by binding of a p107-E2F complex that is disrupted following exposure to IL-3 (60). Further examination of these regulatory pathways in myeloid cells derived from $p107^{-/-}$ mice in a BALB/cJ genetic background should elucidate the molecular basis of the phenomena.

Loss of Rb function is attributed to the development of several cancers, including retinoblastoma in humans and pituitary tumors in mice (61). Although p107 is highly related to Rb, the homozygous loss of p107 function in neoplasia is not well-documented, leading to ambiguity as to whether *p107* can be considered a tumor suppressor protein. In humans, the *p107* gene maps to the long arm of chromosome 20, and 20q deletions are highly prevalent in myeloproliferative disorders, myelodysplastic syndromes, and acute myeloid leukemia (58). However, inconsistent with a tumor suppressor role for p107 is the observation that homozygous loss of p107 occurs only in a small subgroup of myeloid neoplasias associated with loss of 20q (1). Nevertheless, our observations of hyperplastic changes in the myeloid lineage of $p107^{-/-}$ mice suggest that homozygous loss-of-function mutations in *p107* can contribute to the development of myeloid proliferative disorders.

We have also derived a targeted null mutation in *p130* and have bred the mutant allele into either a BALB/cJ or a C57BL/6J genetic background. Strikingly, we observed $p130^{-/-}$ embryos in a background enriched for BALB/cJ die in utero, whereas $p130^{-/-}$ mice in a background enriched for C57BL/6J were viable and exhibited no apparent phenotype (30a). These data strongly support our interpretation that second-site modifier genes that affect the penetrance of null mutations in *p107* or *p130* exist. We are currently assessing whether $Rb^{-/-}$ embryos exhibit an increased severity of phenotype in a BALB/cJ genetic background.

The existence of second-site modifier loci affecting the penetrance of the phenotypes of mice carrying targeted null mutations has been reported by several laboratories. These include targeted mutations in IGF-1, fibronectin, EGF, CFTR, TGFβ1, TGFβ3, and β1-adrenergic receptor (6, 18, 34, 46, 49, 50, 56, 59). The genetic basis for the difference in penetrance

of the *p107*$^{-/-}$ phenotype on C57BL/6J versus BALB/cJ backgrounds remains to be established. The breeding data are consistent with the existence of multiple modifier alleles representing either recessive loss-of-function mutations in the C57BL/6J background, dominant gain-of-function mutations in the BALB/cJ background, or a mixture of both (Table 2). Alternatively, our data do not rule out the possibility that heterozygosity at some modifier alleles contributes to the observed phenotype. In our experiments, we have not directly assessed the role played by the 129/Sv chromosomes segregating in the different offspring. However, genetic analysis should allow a resolution of all of these issues. Currently, we are performing microsatellite analysis to accurately determine the number of modifying genes and to map their approximate locations. Clearly, understanding the identities of the modifier genes having a potentially epistatic relationship with *p107* and *p130* will provide important insights into the regulatory pathways within which p107 and p130 operate.

ACKNOWLEDGMENTS

M.A.R. is a Research Scientist of the National Cancer Institute of Canada and a member of the Canadian Genetic Disease Network of Excellence. We thank John Hassell, Bill Muller, and Peter Whyte for critical reading of the manuscript; Katherine A. Chorneyko and Brian Leiber for histopathology consultations; Ann Dorward for assistance with flow cytometry; Adele Girgis-Gabardo for technical assistance; and Olga Gan and John Dick for performing bone marrow colony assays.

This work was supported by a grant from the National Cancer Institute of Canada to M.A.R.

REFERENCES

1. **Asimakopoulos, F. A., N. J. White, E. Nacheva, and A. R. Green.** 1994. Molecular analysis of chromosome 20q deletions associated with myeloproliferative disorders and myelodysplastic syndromes. Blood **84:**3086–3094.
2. **Baker, J., J. P. Liu, E. J. Robertson, and A. Efstratiadis.** 1993. Role of insulin-like growth factors in embryonic and postnatal growth. Cell **75:**73–82.
3. **Bang, O. S., F. W. Ruscetti, M. H. Lee, S. J. Kim, and M. C. Birchenall-Roberts.** 1996. Transforming growth factor-beta1 modulates p107 function in myeloid cells: correlation with cell cycle progression. J. Biol. Chem. **271:**7811–7819.
4. **Beijersbergen, R. L., E. M. Hijmans, L. Zhu, and R. Bernards.** 1994. Interaction of c-Myc with the pRb-related protein p107 results in inhibition of c-Myc-mediated transactivation. EMBO J. **13:**4080–4086.
5. **Bignon, Y. J., Y. Chen, C. Y. Chang, D. J. Riley, J. J. Windle, P. L. Mellon, and W. H. Lee.** 1993. Expression of a retinoblastoma transgene results in dwarf mice. Genes Dev. **7:**1654–1662.
6. **Bonyadi, M., S. A. Rusholme, F. M. Cousins, H. C. Su, C. A. Biron, M. Farrall, and R. J. Akhurst.** 1997. Mapping of a major genetic modifier of embryonic lethality in TGF beta 1 knockout mice. Nature Genet. **15:**207–211.
7. **Botz, J., K. Zerfass-Thome, D. Spitkovsky, H. Delius, B. Vogt, M. Eilers, A. Hatzigeorgiou, and P. Jansen-Durr.** 1996. Cell cycle regulation of the murine cyclin E gene depends on an E2F binding site in the promoter. Mol. Cell. Biol. **16:**3401–3409.
8. **Brehm, A., E. A. Miska, D. J. McCance, J. L. Reid, A. J. Bannister, and T. Kouzarides.** 1998. Retinoblastoma protein recruits histone deacetylase to repress transcription. Nature **391:**597–601.
9. **Bremner, R., B. L. Cohen, M. Sopta, P. A. Hamel, C. J. Ingles, B. L. Gallie, and R. A. Phillips.** 1995. Direct transcriptional repression by pRB and its reversal by specific cyclins. Mol. Cell. Biol. **15:**3256–3265.
10. **Cao, L., B. Faha, M. Dembski, L. H. Tsai, E. Harlow, and N. Dyson.** 1992. Independent binding of the retinoblastoma protein and p107 to the transcription factor E2F. Nature **355:**176–179.
11. **Chellappan, S. P., S. Hiebert, M. Mudryj, J. M. Horowitz, and J. R. Nevins.** 1991. The E2F transcription factor is a cellular target for the RB protein. Cell **65:**1053–1061.
12. **Chittenden, T., D. M. Livingston, and J. A. DeCaprio.** 1993. Cell cycle analysis of E2F in primary human T cells reveals novel E2F complexes and biochemically distinct forms of free E2F. Mol. Cell. Biol. **13:**3975–3983.
13. **Clarke, A. R., E. R. Maandag, M. van Roon, N. M. van der Lugt, M. van der Valk, M. L. Hooper, A. Berns, and H. te Riele.** 1992. Requirement for a functional Rb-1 gene in murine development. Nature **359:**328–330.
14. **Cobrinik, D., M. H. Lee, G. Hannon, G. Mulligan, R. T. Bronson, N. Dyson, E. Harlow, D. Beach, R. A. Weinberg, and T. Jacks.** 1996. Shared role of the pRB-related p130 and p107 proteins in limb development. Genes Dev. **10:**1633–1644.
15. **DeGregori, J., T. Kowalik, and J. R. Nevins.** 1995. Cellular targets for activation by the E2F1 transcription factor include DNA synthesis- and G_1/S-regulatory genes. Mol. Cell. Biol. **15:**4215–4224.
16. **Fantl, V., G. Stamp, A. Andrews, I. Rosewell, and C. Dickson.** 1995. Mice lacking cyclin D1 are small and show defects in eye and mammary gland development. Genes Dev. **9:**2364–2372.
17. **Geng, Y., E. N. Eaton, M. Picon, J. M. Roberts, A. S. Lundberg, A. Gifford, C. Sardet, and R. A. Weinberg.** 1996. Regulation of cyclin E transcription by E2Fs and retinoblastoma protein. Oncogene **12:**1173–1180.
18. **George, E. L., E. N. Georges-Labouesse, R. S. Patel-King, H. Rayburn, and R. O. Hynes.** 1993. Defects in mesoderm, neural tube and vascular development in mouse embryos lacking fibronectin. Development **119:**1079–1091.
19. **Gu, W., K. Bhatia, I. T. Magrath, C. V. Dang, and R. Dalla-Favera.** 1994. Binding and suppression of the Myc transcriptional activation domain by p107. Science **264:**251–254.
20. **Herrera, R. E., V. P. Sah, B. O. Williams, T. P. Makela, R. A. Weinberg, and T. Jacks.** 1996. Altered cell cycle kinetics, gene expression, and G_1 restriction point regulation in Rb-deficient fibroblasts. Mol. Cell. Biol. **16:**2402–2407.
21. **Hiebert, S. W., S. P. Chellappan, J. M. Horowitz, and J. R. Nevins.** 1992. The interaction of RB with E2F coincides with an inhibition of the transcriptional activity of E2F. Genes Dev. **6:**177–185.
22. **Hoang, A. T., B. Lutterbach, B. C. Lewis, T. Yano, T. Y. Chou, J. F. Barrett, M. Raffeld, S. R. Hann, and C. V. Dang.** 1995. A link between increased transforming activity of lymphoma-derived MYC mutant alleles, their defective regulation by p107, and altered phosphorylation of the c-Myc transactivation domain. Mol. Cell. Biol. **15:**4031–4042.
23. **Huet, X., J. Rech, A. Plet, A. Vie, and J. M. Blanchard.** 1996. Cyclin A expression is under negative transcriptional control during the cell cycle. Mol. Cell. Biol. **16:**3789–3798.
24. **Hurford, R. K., Jr., D. Cobrinik, M. H. Lee, and N. Dyson.** 1997. pRB and p107/p130 are required for the regulated expression of different sets of E2F responsive genes. Genes Dev. **11:**1447–1463.
25. **Jacks, T., A. Fazeli, E. M. Schmitt, R. T. Bronson, M. A. Goodell, and R. A. Weinberg.** 1992. Effects of an Rb mutation in the mouse. Nature **359:**295–300.
26. **Johnson, D. G., and R. Schneider-Broussard.** 1998. Role of E2F in cell cycle control and cancer. Front. Biosci. **3:**d447–d448.
27. **Johnson, D. G., J. K. Schwarz, W. D. Cress, and J. R. Nevins.** 1993. Expression of transcription factor E2F1 induces quiescent cells to enter S phase. Nature **365:**349–352.
28. **Kablar, B., K. Krastel, C. Ying, A. Asakura, S. J. Tapscott, and M. A. Rudnicki.** 1997. MyoD and Myf-5 differentially regulate the development of limb versus trunk skeletal muscle. Development **124:**4729–4738.
29. **Kim, K. K., M. H. Soonpaa, H. Wang, and L. J. Field.** 1995. Developmental expression of p107 mRNA and evidence for alternative splicing of the p107 (RBL1) gene product. Genomics **28:**520–529.

29a. **LeCouter, J. E., and M. A. Rudnicki.** Unpublished observation.

30. **LeCouter, J. E., P. F. Whyte, and M. A. Rudnicki.** 1996. Cloning and expression of the Rb-related mouse p130 mRNA. Oncogene **12:**1433–1440.

30a. **LeCouter, J. E., B. Kablar, P. F. M. Whyte, C. Ying, and M. A. Rudnicki.** Strain-dependent embryonic lethality in mice lacking the retinoblastoma-related p130 gene. Development, in press.

31. **Lee, E. Y., C. Y. Chang, N. Hu, Y. C. Wang, C. C. Lai, K. Herrup, W. H. Lee, and A. Bradley.** 1992. Mice deficient for Rb are nonviable and show defects in neurogenesis and haematopoiesis. Nature **359:**288–294.
32. **Lee, M. H., B. O. Williams, G. Mulligan, S. Mukai, R. T. Bronson, N. Dyson, E. Harlow, and T. Jacks.** 1996. Targeted disruption of p107: functional overlap between p107 and Rb. Genes Dev. **10:**1621–1632.
33. **Li, E., T. H. Bestor, and R. Jaenisch.** 1992. Targeted mutation of the DNA methyltransferase gene results in embryonic lethality. Cell **69:**915–926.
34. **Liu, J. P., J. Baker, A. S. Perkins, E. J. Robertson, and A. Efstratiadis.** 1993. Mice carrying null mutations of the genes encoding insulin-like growth factor I (Igf-1) and type 1 IGF receptor (Igf1r). Cell **75:**59–72.
35. **Lukas, J., B. O. Petersen, K. Holm, J. Bartek, and K. Helin.** 1996. Deregulated expression of E2F family members induces S-phase entry and overcomes p16INK4A-mediated growth suppression. Mol. Cell. Biol. **16:**1047–1057.
36. **Luo, R. X., A. A. Postigo, and D. C. Dean.** 1998. Rb interacts with histone deacetylase to repress transcription. Cell **92:**463–473.
37. **Magnaghi-Jaulin, L., R. Groisman, I. Naguibneva, P. Robin, S. Lorain, J. P. Le Villain, F. Troalen, D. Trouche, and A. Harel-Bellan.** 1998. Retinoblastoma protein represses transcription by recruiting a histone deacetylase. Nature **391:**601–605.
38. **Maniatis, T., E. F. Fritsch, and J. Sambrook.** 1982. Molecular cloning: a laboratory manual. Cold Spring Harbor Laboratory Press, Cold Spring Harbor, N.Y.
39. **McBurney, M. W., L. C. Sutherland, C. N. Adra, B. Leclair, M. A. Rudnicki, and K. Jardine.** 1991. The mouse Pgk-1 gene promoter contains an upstream activator sequence. Nucleic Acids Res. **19:**5755–5761.
40. **Megeney, L. A., B. Kablar, K. Garrett, J. E. Anderson, and M. A. Rudnicki.**

1996. MyoD is required for myogenic stem cell function in adult skeletal muscle. Genes Dev. **10:**1173–1183.
41. **Muller, R.** 1995. Transcriptional regulation during the mammalian cell cycle. Trends Genet. **11:**173–178.
42. **Mulligan, G., and T. Jacks.** 1998. The retinoblastoma gene family: cousins with overlapping interests. Trends Genet. **14:**223–229.
43. **Nevins, J. R., G. Leone, J. DeGregori, and L. Jakoi.** 1997. Role of the Rb/E2F pathway in cell growth control. J. Cell Physiol. **173:**233–236.
44. **Ohtani, K., J. DeGregori, and J. R. Nevins.** 1995. Regulation of the cyclin E gene by transcription factor E2F1. Proc. Natl. Acad. Sci. USA **92:**12146–12150.
45. **Porcu, P., X. Grana, S. Li, J. Swantek, A. De Luca, A. Giordano, and R. Baserga.** 1994. An E2F binding sequence negatively regulates the response of the insulin-like growth factor 1 (IGF-I) promoter to simian virus 40T antigen and to serum. Oncogene **9:**2125–2134.
46. **Proetzel, G., S. A. Pawlowski, M. V. Wiles, M. Yin, G. P. Boivin, P. N. Howles, J. Ding, M. W. Ferguson, and T. Doetschman.** 1995. Transforming growth factor-beta 3 is required for secondary palate fusion. Nature Genet. **11:**409–414.
47. **Qin, X. Q., D. M. Livingston, M. Ewen, W. R. Sellers, Z. Arany, and W. G. Kaelin, Jr.** 1995. The transcription factor E2F-1 is a downstream target of RB action. Mol. Cell. Biol. **15:**742–755.
48. **Robertson, E. J.** 1987. Embryo-derived stem cells, p. 71–112. *In* E. J. Robertson (ed.), Teratomas and embryonic stem cells: a practical approach. IRL Press, Oxford, United Kingdom.
49. **Rohrer, D. K., K. H. Desai, J. R. Jasper, M. E. Stevens, D. P. Regula, Jr., G. S. Barsh, D. Bernstein, and B. K. Kobilka.** 1996. Targeted disruption of the mouse beta 1-adrenergic receptor gene: developmental and cardiovascular effects. Proc. Natl. Acad. Sci. USA **93:**7375–7380.
50. **Rozmahel, R., M. Wilschanski, A. Matin, S. Plyte, M. Oliver, W. Auerbach, A. Moore, J. Forstner, P. Durie, J. Nadeau, C. Bear, and L. C. Tsui.** 1996. Modulation of disease severity in cystic fibrosis transmembrane conductance regulator deficient mice by a secondary genetic factor. Nature Genet. **12:**280–287.
51. **Rudnicki, M. A., T. Braun, S. Hinuma, and R. Jaenisch.** 1992. Inactivation of MyoD in mice leads to up-regulation of the myogenic HLH gene Myf-5 and results in apparently normal muscle development. Cell **71:**383–390.
52. **Schulze, A., K. Zerfass, D. Spitkovsky, S. Middendorp, J. Berges, K. Helin, P. Jansen-Durr, and B. Henglein.** 1995. Cell cycle regulation of the cyclin A gene promoter is mediated by a variant E2F site. Proc. Natl. Acad. Sci. USA **92:**11264–11268.
53. **Sellers, W. R., J. W. Rodgers, and W. G. Kaelin, Jr.** 1995. A potent transrepression domain in the retinoblastoma protein induces a cell cycle arrest when bound to E2F sites. Proc. Natl. Acad. Sci. USA **92:**11544–11548.
54. **Shan, B., and W. H. Lee.** 1994. Deregulated expression of E2F-1 induces S-phase entry and leads to apoptosis. Mol. Cell. Biol. **14:**8166–8173.
55. **Shirodkar, S., M. Ewen, J. A. DeCaprio, J. Morgan, D. M. Livingston, and T. Chittenden.** 1992. The transcription factor E2F interacts with the retinoblastoma product and a p107-cyclin A complex in a cell cycle-regulated manner. Cell **68:**157–166.
56. **Sibilia, M., and E. F. Wagner.** 1995. Strain-dependent epithelial defects in mice lacking the EGF receptor. Science **269:**234–238.
57. **Sladek, T. L.** 1997. E2F transcription factor action, regulation and possible role in human cancer. Cell Prolif. **30:**97–105.
58. **Testa, J. R., A. Kinnealey, J. D. Rowley, D. W. Golde, and D. Potter.** 1978. Deletion of the long arm of chromosome 20 [del(20)(q11)] in myeloid disorders. Blood **52:**868–877.
59. **Threadgill, D. W., A. A. Dlugosz, L. A. Hansen, T. Tennenbaum, U. Lichti, D. Yee, C. LaMantia, T. Mourton, K. Herrup, R. C. Harris, et al.** 1995. Targeted disruption of mouse EGF receptor: effect of genetic background on mutant phenotype. Science **269:**230–234.
60. **Watanabe, S., S. Ishida, K. Koike, and K. Arai.** 1995. Characterization of cis-regulatory elements of the c-myc promoter responding to human GM-CSF or mouse interleukin 3 in mouse proB cell line BA/F3 cells expressing the human GM-CSF receptor. Mol. Biol. Cell **6:**627–636.
61. **Weinberg, R. A.** 1995. The retinoblastoma protein and cell cycle control. Cell **81:**323–330.
62. **Whyte, P.** 1995. The retinoblastoma protein and its relatives. Semin. Cancer Biol. **6:**83–90.
63. **Williams, B. O., L. Remington, D. M. Albert, S. Mukai, R. T. Bronson, and T. Jacks.** 1994. Cooperative tumorigenic effects of germline mutations in Rb and p53. Nature Genet. **7:**480–484.
64. **Zerfass-Thome, K., A. Schulze, W. Zwerschke, B. Vogt, K. Helin, J. Bartek, B. Henglein, and P. Jansen-Durr.** 1997. p27KIP1 blocks cyclin E-dependent transactivation of cyclin A gene expression. Mol. Cell. Biol. **17:**407–415.